Neurosci. Bull.
https://doi.org/10.1007/s12264-022-00951-5

www.neurosci.cn
www.springer.com/12264

ORIGINAL ARTICLE

Disrupted Maturation of Prefrontal Layer 5 Neuronal Circuits in an Alzheimer's Mouse Model of Amyloid Deposition

Chang Chen[1,2] · Jing Wei[2] · Xiaokuang Ma[2] · Baomei Xia[2] · Neha Shakir[2] · Jessica K. Zhang[2] · Le Zhang[2] · Yuehua Cui[2] · Deveroux Ferguson[2] · Shenfeng Qiu[2] · Feng Bai[1]

Received: 26 April 2022 / Accepted: 18 June 2022

Abstract Mutations in genes encoding amyloid precursor protein (APP) and presenilins (PSs) cause familial forms of Alzheimer's disease (AD), a neurodegenerative disorder strongly associated with aging. It is currently unknown whether and how AD risks affect early brain development, and to what extent subtle synaptic pathology may occur prior to overt hallmark AD pathology. Transgenic mutant APP/PS1 over-expression mouse lines are key tools for studying the molecular mechanisms of AD pathogenesis. Among these lines, the 5XFAD mice rapidly develop key features of AD pathology and have proven utility in studying amyloid plaque formation and amyloid β (Aβ)-induced neurodegeneration. We reasoned that transgenic mutant APP/PS1 over-expression in 5XFAD mice may lead to neurodevelopmental defects in early cortical neurons, and performed detailed synaptic physiological characterization of layer 5 (L5) neurons from the prefrontal cortex (PFC) of 5XFAD and wild-type littermate controls. L5 PFC neurons from 5XFAD mice show early APP/Aβ immunolabeling. Whole-cell patch-clamp recording at an early post-weaning age (P22–30) revealed functional impairments; although 5XFAD PFC-L5 neurons exhibited similar membrane properties, they were intrinsically less excitable. In addition, these neurons received smaller amplitude and frequency of miniature excitatory synaptic inputs. These functional disturbances were further corroborated by decreased dendritic spine density and spine head volumes that indicated impaired synapse maturation. Slice biotinylation followed by Western blot analysis of PFC-L5 tissue revealed that 5XFAD mice showed reduced synaptic AMPA receptor subunit GluA1 and decreased synaptic NMDA receptor subunit GluN2A. Consistent with this, patch-clamp recording of the evoked L23>L5 synaptic responses revealed a reduced AMPA/NMDA receptor current ratio, and an increased level of AMPAR-lacking silent synapses. These results suggest that transgenic mutant forms of APP/PS1 overexpression in 5XFAD mice leads to early developmental defects of cortical circuits, which could contribute to the age-dependent synaptic pathology and neurodegeneration later in life.

Keywords Alzheimer's disease · Mouse model · Synaptic plasticity · Long-term potentiation · Cortical circuit · Electrophysiology · Learning and memory

Introduction

Alzheimer's disease (AD) is the most frequent form of dementia. A hallmark pathology of the AD brain is the degenerating cortical neurons overloaded with neurofibrillary tangles and amyloid plaques [1]. At the cellular and functional levels, early AD brain pathology is characterized by impaired synaptic function and synapse loss, manifested as disrupted synaptic plasticity, learning, memory, and cognition [2–4]. Transgenic mice that overexpress mutated human amyloid precursor protein (APP), presenilin, and tau genes reproduce many aspects of AD pathology such as amyloid β (Aβ) plaques, neurofibrillary tangles, reactive gliosis, and synaptic and neuronal loss, which are consistent with behavioral changes such as progressive age-dependent memory impairments [5, 6]. As such, these

✉ Shenfeng Qiu
sqiu@arizona.edu

✉ Feng Bai
baifeng515@126.com

[1] Department of Neurology, Affiliated Drum Tower Hospital, Medical School of Nanjing University, Nanjing 210008, China

[2] Basic Medical Sciences, University of Arizona College of Medicine-Phoenix, Phoenix, AZ 85004, USA

Published online: 24 September 2022

mouse lines are useful to inform the molecular and cellular changes associated with AD.

The 5XFAD mouse line, which co-overexpresses human APP and presenilin 1 (PS1) harboring five familial AD mutations manifest very early-onset and aggressive amyloid deposition [7, 8]. These mice start to develop amyloid plaques as early as ~2 months of age, when they show dramatically accelerated intraneuronal Aβ42 production. Pathologically, Aβ deposition emerges in the hippocampal subiculum and in layer 5 (L5) principal neurons of the neocortex, and rapidly increases in affected brain regions [7, 9]. Synaptic failure reportedly takes place prior to overt plaque formation; for example, hippocampal basal synaptic transmission and theta burst stimulus-induced LTP are impaired at 6 months, but not prior to 4 months [10]. In addition, synaptic failure manifests at multiple levels, ranging from functional alterations to structural disturbances [11]. Synaptic failure of L5 neurons in 5xFAD mice reportedly long precedes the physical loss of synapses, which occurs by 12 months of age [11].

Although AD is considered to be an aging-related neurodegenerative disorder, mutant forms of APP/PS1 are expressed throughout the life span. How transgenic over-expression of these mutant forms affects the developing neural circuits remain an outstanding question. The 5XFAD mouse line, in which the thy1 promoter is used to drive very early transgenic APP/PS1 expression in the brain, offers a unique opportunity to study neurodevelopmental effects of mutant APP/PS1 over-loading in the affected neuron populations [7]. Despite a large literature exploring the mechanisms of neurodegeneration in 5XFAD mice [12–15], no study has explored the potential developmental sequelae of mutant APP/PS1 early on in vulnerable cortical circuits. As the thy1-promotor-driven expression of mutated forms of APP/PS1 is expected to predominantly affect L5 neurons [11, 16, 17], we reasoned that these mutated forms may have a detrimental effect at an early developmental time point, thus impairing the normal trajectory of synapse function and connectivity. In this study, we provide electrophysiology evidence of altered intrinsic excitability and impaired synaptic activity, as well as disrupted synaptic glutamate receptor content and functional glutamatergic synapses in L5 PFC neurons at an early post-weaning age (P22–28). To the best of our knowledge, this study reveals some of the earliest synaptic functional alterations, and suggests negative neurodevelopmental sequelae as an underappreciated neuropathology in this prominent AD mouse model.

Materials and Methods

Animals and Disease Model

The 5XFAD mice used in this study were purchased from the Jackson Laboratory (catalog #34848-JAX). This line overexpresses both the human amyloid precursor protein (*APP*) gene with K670N/M671L, V717I, and I716V mutations and the human *PS1* M146L and L286V mutations under the Thy1 promoter [7]. Mice were genotyped according to the JAX protocol using three primers (mutant, AAG CTA GCT GCA GTA ACG CCA TTT; wild type, ACC TGC ATG TGA ACC CAG TAT TCT ATC; and common, CTA CAG CCC CTC TCC AAG GTT TAT AG). Mice were weaned at P21 and used for experiments on postnatal days 22–28. All experimental procedures conformed to NIH guidelines and were approved by the Institutional Animal Care and Use Committee of the University of Arizona and the Animal Care and Use Committee of the Model Animal Research Center, Nanjing University.

Immunohistochemistry/Immunofluorescence

Mice were anesthetized with 4% isoflurane and transcardially perfused with 0.01mol/L PBS, followed by cold 4% paraformaldehyde (PFA) formulated in 0.1 mol/L phosphate buffer (pH 7.4). Brains were post-fixed in cold 4% PFA overnight at 4°C, and cryoprotected in 30% sucrose for 2 days. The brains were then embedded in OCT, and cut into 40-μm frozen sections on a sliding microtome (Leica SR-2000). The sections were washed three times in 0.01 mol/L PBS, and permeabilized in PBS-0.2% Triton. For APP/Aβ staining, free-floating sections were blocked in primary antibody dilution solution (0.2% Triton, 5% normal goat serum, and 1% bovine serum albumin in 0.01 mol/L PBS) for 2 h, and incubated with anti-APP/Aβ primary antibody (clone 6E10, Biolegend, Cat# SIG-39320. Antibody Registry ID: AB_662798. 1:500 dilution) for 24 h, followed by Alexa 555-conjugated goat anti-mouse antibody. For APP/Aβ, Iba1, and Thio-S triple staining, sections were similarly blocked in primary antibody dilution solution, and incubated with anti-APP/Aβ (6E10) and anti-Iba1 (#019-19741, Wako, 1:500 dilution) primary antibodies for 24 h. After incubation with A555-conjugated goat anti-mouse and A488-conjugated goat anti-rabbit antibodies for 24 h, sections were extensively washed in 0.01 mol/L PBS, and further stained with 0.025% Thio-S (prepared in 50% ethanol–50% PBS) for 10 min. These sections were mounted on SuperFrost Plus slides (VWR Scientific, West Chester, PA) using DAPI-containing Vectashield mounting medium (H-1200, Vector Laboratories). Images were captured on an LSM 710 confocal microscope (Zeiss GmbH, Germany) with appropriate laser lines and filters.

Whole-Cell Patch-Clamp Recording in Brain Slices

Whole-cell recordings were made in L5 pyramidal neurons in parasagittal PFC slices. Mice of desired genotypes were

anesthetized using 3%–5% isoflurane. To improve slice viability, intra-cardiac perfusion of ice-cold choline solution (in mmol/L: 110 choline chloride, 25 $NaHCO_3$, 2.5 KCl, 1.25 NaH_2PO_4, 0.5 $CaCl_2$, 7 $MgSO_4$, 25 D-glucose, 11.6 sodium ascorbate, and 3.1 sodium pyruvate, saturated with 95% O_2 / 5% CO_2) was perfused before mice were decapitated and brains quickly dissected out. To prepare PFC slices (350 µm thick), we used parasagittal sections, which allows better preservation of intracortical synaptic connectivity [18]. Slices were cut in ice-cold choline solution on a vibratome (VT-1200S, Leica). PFC slices were kept in artificial cerebrospinal fluid (ACSF, containing in mmol/L: 126 NaCl, 2.5 KCl, 26 $NaHCO_3$, 2 $CaCl_2$, 2 $MgCl_2$, 1.25 NaH_2PO_4, and 10 D-glucose; saturated with 95% O_2 / 5% CO_2) for 30 min at 35°C, and then maintained at 24°C (room temperature) until recording.

The brain slices were transferred to a customized submerged chamber and perfused with ACSF saturated with 95% O_2 / 5% CO_2. Slices were visualized under a 4× objective (Olympus UPlanApo, NA = 0.16) to locate the cyto-architectural landmarks of layer 5. To minimize neurite cutoffs, only L5 pyramidal neurons with a soma at least 50 µm below the slice surface were selected for whole-cell recordings. Neuronal somas were identified and targeted using a 60× objective (NA = 0.9) under IR illumination (Olympus BX-51 WI microscope). Neuronal signals were amplified using a MultiClamp 700B amplifier (Molecular Devices, Forster City, CA), low-pass filtered at 1 kHz (voltage clamp) or 10 kHz (current clamp), and digitized at 20 kHz using a Digidata 1440A interface controlled by pClamp 10.6 (Molecular Devices). Neuronal membrane properties (input resistance and capacitance) were measured as current responses to +/– 5mV voltage steps. Intrinsic excitability was quantified as the number of action potentials elicited by current injection (–100 to 500 pA in 50-pA steps). To record mEPSCs, D-AP5 (50 µmol/L, Tocris) and tetrodotoxin (TTX, 1 µmol/L, Tocris) were added to the circulating ACSF. The electrode internal solution contained (in mmol/L): 130 K-gluconate, 10 HEPES, 4 KCl, 4 ATP-Mg, 0.3 GTP-Na, 2 NaCl, 1 EGTA, and 14 phosphocreatine (pH 7.2, 295–300 mOsm). To record miniature inhibitory postsynaptic currents (mIPSCs), the ACSF contained 1 µmol/L TTX and 10 µmol/L CNQX, and the electrode internal solution consisted (in mmol/L): 125 KCl, 2.8 NaCl, 2 $MgCl_2$, 0.3 Na_3GTP, 2 Mg^{2+}-ATP, 1 EGTA, 10 HEPES, and 10 phosphocreatine (pH 7.25, ~300 mOsm). In some mEPSC/mIPSC recording experiments, 0.15% biocytin (W/V) was included in the recording electrode to reveal neuronal morphology. During the recordings, series resistance (Rs, <25 MΩ) was constantly monitored and neurons with >20% variations in Rs were excluded from analyses.

To measure the AMPA/NMDA receptor current ratio (A:N) in L5 PFC neurons, a bipolar stimulating electrode (FHC, Bowdoin, ME) was placed in L2/3 of the PFC. A Cs+-based internal solution (containing in mmol/L, 125 Cs-gluconate, 5 TEA-Cl, 10 HEPES, 2.5 CsCl, 8 NaCl, 5 QX314-HCl, 4 Mg^{2+}-ATP, 0.3 Na_3GTP, 1 EGTA and 10 phosphocreatine, pH 7.25) was used. Evoked monosynaptic responses were obtained when neurons were sequentially voltage-clamped at –70 mV (for AMPAR-mediated synaptic currents) and +40 mV (AMPAR+NMDAR currents). The A:N ratio was quantified using the peak of EPSC amplitude at –70 mV (AMPAR current), and +40 mV (NMDAR current, which was measured at 75 ms after stimulus onset [19]).

To estimate the proportion of silent synapses in the L2/3 to L5 mPFC circuit, we used a minimum stimulation protocol to activate a small number of axons (release sites) by placing a theta glass electrode in L2/3. L5 neurons were first voltage-clamped at –70 mV using the Cs-based internal solution described above. A minimum stimulus intensity that produced interleaved success and failure of AMPAR EPSCs at −70 mV was applied and kept constant. After collecting 200 trials (inter-trial interval, 2 s), neurons were voltage-clamped at +40 mV to collect 200 more trials. The percentage of NMDAR-only silent synapses was calculated from the difference in failure rates of AMPAR-EPSCs (–70 mV) and compound-EPSCs (+40 mV) [20–22].

Surface Protein Biotinylation and Western Blot Analysis

To assess total glutamate receptor protein levels and their membrane-bound fractions at synaptic sites, P25–28 acute PFC slices were treated with 0.25 mg/mL sulfo-NHS-S-S-biotin for 30 min at 4°C, using a Piece^{TM} cell surface protein isolation kit (ThermoFisher Scientific, cat# 89881), similar to that described previously for biotinylation in slices [21, 23]. Micro-dissected PFC-L5 tissue (pooled from 2–3 mice) was homogenized on ice in buffer (containing 320 mmol/L sucrose, 4 mmol/L HEPES, and 1:50 protease inhibitor mixture; P8340, Sigma-Aldrich). The homogenates were centrifuged at 1500× *g* for 10 min, after which the supernatant was collected and centrifuged at 16,000× *g* for 20 min to pellet the crude synaptosome fraction, which was further equally divided into two aliquots. One aliquot was used to assess total synaptosomal proteins, while the other was lysed and re-suspended in ice-cold water supplemented with the protease inhibitor mixture (P8340, Sigma-Aldrich). NeutraAvidin beads (ThermoFisher) were then added to capture biotinylated synaptic proteins by rotation of the sample for 2 h at 4°C. The beads were washed three times in RIPA buffer, and the biotinylated synaptic membrane proteins were eluted with 2× Laemmli buffer (supplemented with 50 µmol/L DTT). The biotinylated proteins were separated

by SDS-PAGE, and subjected to Western blot analysis using specific antibodies against glutamate receptor subunits.

A standard Western blot protocol was applied to quantify proteins. Total synaptic protein or synaptic surface protein samples were mixed with an equal amount of 2× Laemmli loading buffer and boiled for 5 min, then separated on 4%–15% SDS-polyacrylamide gels. Proteins were then transferred to PVDF membranes (Immobilon-P, Sigma-Aldrich), incubated overnight at 4°C with antibodies against several glutamate receptor subunits that were diluted in 5% nonfat dry milk. The PVDF membranes were then washed three times in 0.01 mol/L PBS-Tween 20, followed by a 2-h incubation with HRP-conjugated secondary antibodies (Jackson ImmunoResearch). Protein signals were developed using an enhanced chemiluminescence method (SignalFire, Cell Signaling Technology), and captured on ECL Hyperfilm (Amersham). The antibodies used in this study were, rabbit anti-GluA1 (AB5849) from Millipore/Chemicon and rabbit anti-GluN2A (#4205), rabbit anti-GluN2B (#14544), rabbit anti-GAPDH (#5174), and rabbit anti-GluN1 (#5704) from Cell Signaling Technology. The final dilution of antibodies was between 1:1000 and 1:2000. The optical density of protein signal bands on Hyperfilm was quantified by densitometry using ImageJ/FIJI.

Neuronal Morphology

Recorded PFC-L5 neuronal morphology, including dendritic arborization and spine morphometric measures, were analyzed as described previously [21, 24]. After completion of whole-cell recording, neurons were injected with 500 pA current to facilitate biocytin diffusion into the neurite processes. The slices were then fixed in 4% PFA overnight, blocked with 1% BSA/0.01 mol/L PBS, and permeabilized with 0.2% Triton X-100. Slices were further incubated with avidin-Alexa 488 for 24 h and mounted on glass slides with a pair of ~350-μm spacers to prevent tissue crushing. Neuronal dendritic arbors were reconstructed after collecting Z-stack images on a confocal microscope (Zeiss LSM 710). The maximal projection images were then imported into FIJI/ImageJ, and neurite arborization and Sholl analysis [25] were done using the Simple Neurite Tracer plugin [26]. This allows quantification of morphometric features such as dendritic arbor, length, and number of intersections as a function of distances from soma. To analyze spines, Z stacks of spines from the apical dendrites (200–450 μm from the soma, secondary branches) were collected with a 63× objective (Plan-Apochromat, NA 1.4). Each Z stack was collected at 512 × 512 pixels, with 4× digital zoom and 0.2-μm Z step size. Imaris software (V8.02, Bitplane, South Windsor, CT) was used to measure spine length, density, and head volume, as we described previously [21, 24].

Statistical Analyses

All results are reported as the mean ± SEM. (standard error of the mean). The experimenters were blinded to genotypes/grouping during data collection and analyses. Sample sizes and numbers of independent experiments were estimated by power analyses using an R script ('pwr' package in CRAN) that takes pre-specified effect size, and type I and II errors as input arguments. Sex-segregated data were first analyzed for potential sex-specific effects, and pooled together for grouped analyses. The Shapiro–Wilk test and F test were first applied to test normality and equal variance. For normally-distributed/equal-variance data, Student's t test or one/two-way analysis of variation was used; for non-normally distributed/ordinal data types, the nonparametric Mann-Whitney U test or Kolmogorov–Smirnov (K-S) test was used. The K-S test was used to compare the cumulative distributions of mEPSC amplitudes. Statistical analyses and graphing were applied using GraphPad Prism 8.0, Microsoft Excel and MATLAB. Figures were prepared using Adobe Creative Cloud. $P < 0.05$ was considered statistically significant for all tests.

Results

APP/Aβ Overload in PFC L5 Neurons During Early Postnatal Development

It has been shown that 5XFAD mice exhibit robust Aβ pathology with onset of extracellular plaque pathology at ~2 months of age, and manifest abundant intraneuronal and plaque-associated changes as early as 3 months of age [7]. Because thy1 promoter-driven transgenic APP/PS1 expression is enriched in cortical L5 neurons and occurs across life span [16, 17], we asked whether the intraneuronal APP/Aβ load can be detected in cortical L5 neurons at very early developmental stages. We applied IHC staining to detect APP/Aβ (6E10 antibody) [27], and found that at postnatal day P21, in most cortical regions including the PFC and retrosplenial cortex, L5 neurons showed APP/Aβ immunoreactivity, which was stronger than in CA1 neurons (Fig. 1A). In addition, we observed strong APP/Aβ immunoreactivity in the subiculum region in the temporal levels of the hippocampus, consistent with reports that the subiculum is one of earliest structure to show APP/Aβ deposition [7]. APP/Aβ overloading in L5 neuron at this early age was associated with a small number of Iba1-positive activated microglia (Fig. 1B). Importantly, at this early age, no extracellular amyloid plaques or Thio-S+ insoluble fibrillar dense core Aβ deposits were observed. In contrast, PFC L5 neurons in 5-month-old (P150) 5XFAD mice showed extensive APP/Aβ immunoreactivity, substantial Aβ plaque deposition that

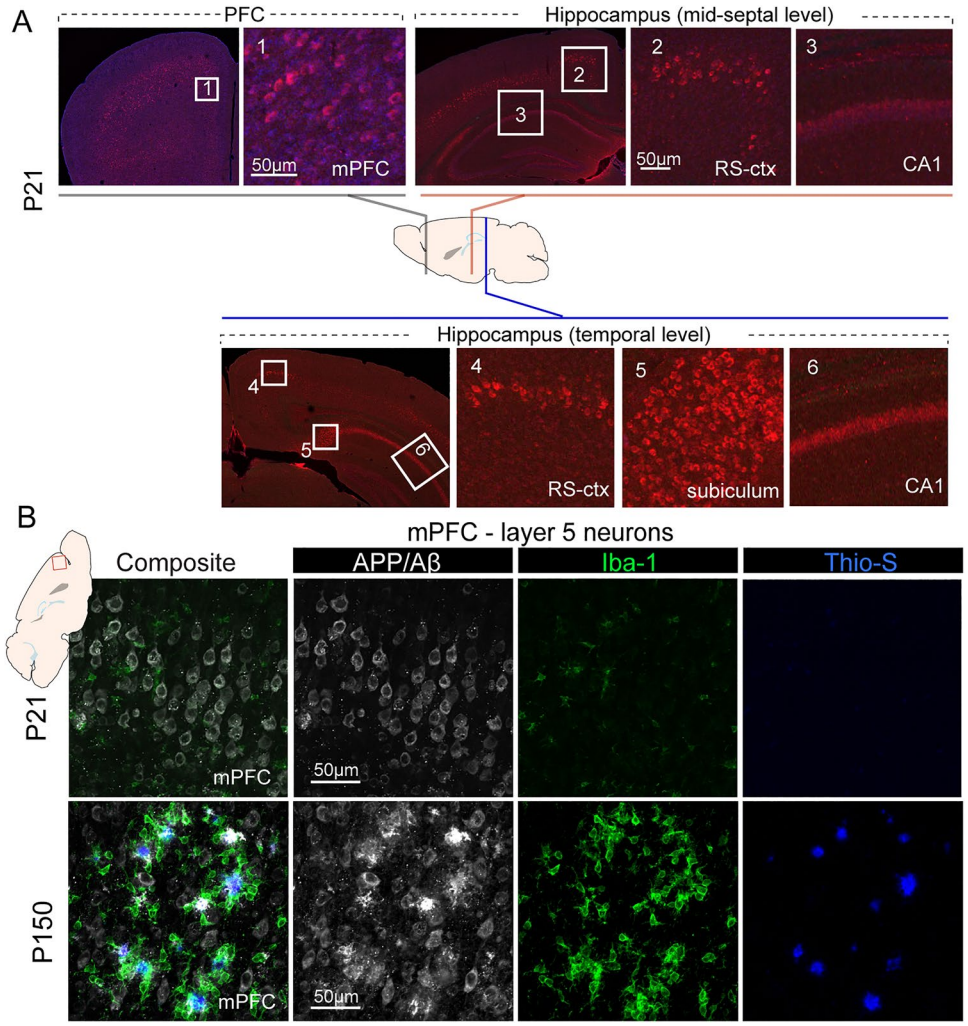

Fig. 1 Age-dependent transgenic APP/Aβ overloading and pathology in the PFC. **A** IHC using 6E10 antibody reveals extensive L5 intraneuronal labeling of APP/Aβ in prefrontal cortex (left) and to a lesser extent, in the retrosplenium cortex (RS-ctx). CA1 neurons also show relatively weaker APP/Aβ immunoreactivity. In comparison, hippocampal subiculum and CA1 neurons at the temporal levels along the septo-temporal axis show stronger APP/Aβ immunoreactivity. **B** Triple IHC staining of APP/Aβ, Iba1, and Thio-S to label amyloid deposition, reactive microglia, and dense-core fibrillar amyloid plaques. L5 neurons of P21 PFC show strong intracellular APP/Aβ labeling, with minimum reactive microglia and no Thio-S+ plaque deposition. In contrast, L5 neurons from P150 mPFC show strong extracellular amyloid deposition with dense Thio-S+ fibrillar Aβ cores that are surrounded by large numbers of Iba1+ reactive microglia.

was surrounded by clustered Iba-1+ reactive microglia, and profound Thio-S-labeled dense-core fibrillar amyloid deposits (Fig. 1B). Notably, the APP/Aβ intracellular overloading in PFC-L5 neurons was also seen at earlier ages (P11 and P14, data not shown), indicating that transgenic expression of mutant APP/PS1 is a continuous process that spans early cortical development.

Decreased Intrinsic Excitability in PFC-L5 Neurons

The early APP/Aβ overloading in PFC-L5 neurons justified investigation on the functional alterations in these affected neurons. We conducted whole-cell patch-clamp recording in PFC-L5 pyramidal neurons to probe potential functional alterations. Parasagittal brain slices containing the PFC were prepared from P22–28 5XFAD mice and their WT littermate controls. We first measured the membrane properties of L5 neurons (Fig. 2A), and found that 5XFAD neurons had similar input resistance (WT, 280.5 ± 20.4 MΩ; 5XFAD, 310.3 ± 19.6 MΩ. $t_{16} = 1.03$, $P = 0.32$) and membrane capacitance (WT, 66.6 ± 3.2 pF; 5XFAD, 66.9 ± 3.6 pF, $t_{16} = 0.05$, $P = 0.96$). 5XFAD PFC-L5 neurons did not show a change in action potential (AP) spike frequency adaptation (Fig. 2B. WT, 0.82 ± 0.03; 5XFAD, 0.81±0.02, $t_{13} = 0.23$, $P = 0.83$). In addition, neurons from both groups exhibited a similar AP half-width (Fig. 2C. WT, 1.34 ± 0.04 ms; 5XFAD, 1.38 ± 0.04 ms. $t_{14} = 0.69$, $P = 0.50$), and the slope of AP depolarization/repolarization, as evidenced by the overlapping 95% confidence intervals of the phase plot (dV/dt *vs* Vm).

PFC-L5 neurons from 5XFAD and WT brain slices were next injected with current steps from –100 to 500 pA in 50-pA increment to test their intrinsic excitability. Fig. 2D shows two representative AP firing responses from WT and 5XFAD neurons in response to each current step injection. Comparing the responses from all neurons (WT, $n = 4$; 5XFAD, $n = 4$) revealed that 5XFAD neurons were intrinsically less excitable, with a smaller number of AP responses to current steps (Fig. 2E. Repeated measures two-way ANOVA, genotype effects: $F_{(1,6)} = 10.9$, $P = 0.016$). For both 5XFAD and WT control neurons, a representative

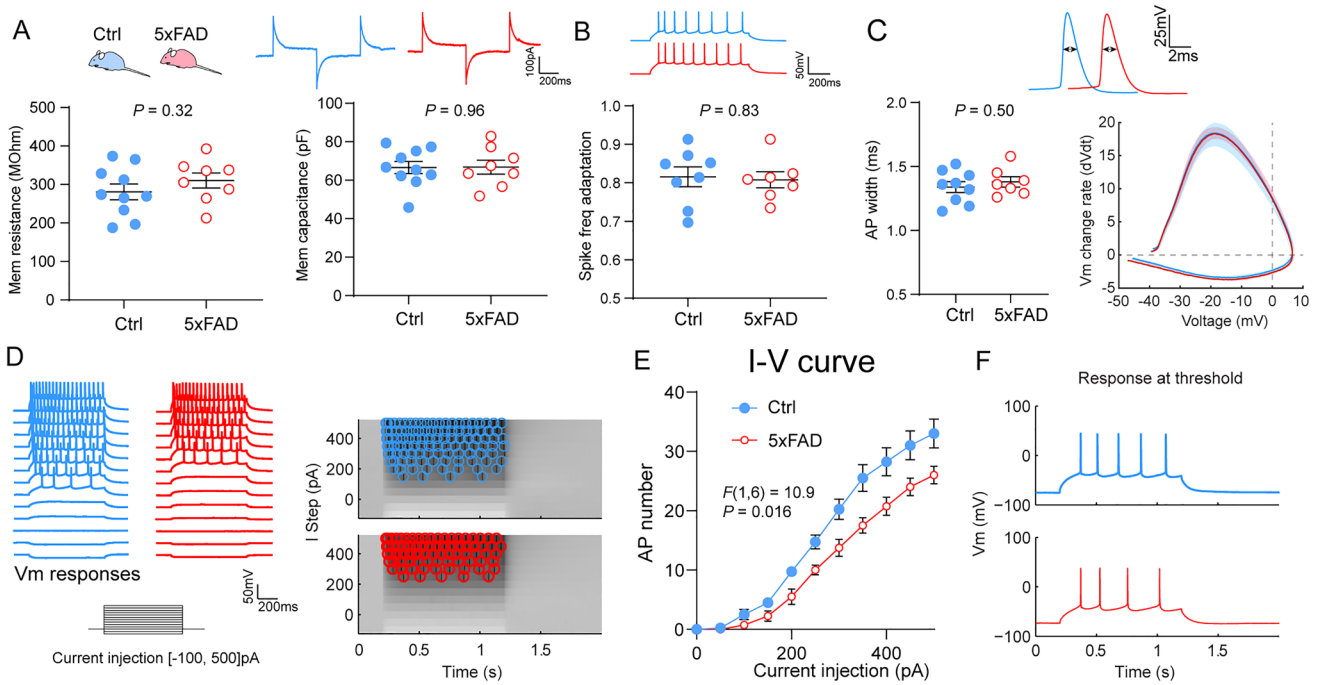

Fig. 2 PFC- L5 neurons in 5XFAD mice exhibit reduced intrinsic excitability. **A** Compared with control littermate neurons, PFC-L5 neurons from 5XFAD brain slices show similar membrane input resistance (t_{16} = 1.03, P = 0.32) and membrane capacitance (t_{16} = 0.05, P = 0.96). Representative current responses to voltage steps are shown above, based on which membrane properties were calculated. **B** 5XFAD PFC-L5 neurons exhibit similar spike frequency adaptation (t_{13} = 0.23, P = 0.83). **C** 5XFAD neurons show similar action potential half-width (t_{14} = 0.69, P = 0.50), and the slope of AP depolarization/repolarization, as evidenced by the overlapping 95% confidence intervals of the phase plot (dV/dt *vs* Vm). **D** Representative intrinsic excitability responses and AP density plot from control and 5XFAD neurons in response to current-step injections (−100 to 500 pA ay 50-pA increments). **E** Pooled data demonstrate that 5XFAD neurons show significantly lower firing rates (genotype effects: F(1,6) = 10.9, P = 0.016. Repeated measures two-way ANOVA). **F** Representative AP firing responses to threshold current step injection in control and 5XFAD neurons.

AP firing response to threshold current step injection is presented in Fig. 2F. These data indicate that PFC-L5 neurons in 5XFAD slices are intrinsically less excitable as a result of developmental transgenic overexpression of mutant APP/PS1.

Reduced Excitatory Synaptic Transmission in PFC-L5 Neurons at 3–4 Weeks Age

We next asked whether developmental intracellular APP/Aβ overloading changes the synaptic activity of PFC-L5 neurons at an early post-weaning age. Whole-cell patch-clamp recording was used to first measure miniature excitatory postsynaptic currents (mEPSC) in slices prepared from P22–28 5XFAD and WT littermate mice. Representative mEPSC traces from both groups are shown in Fig. 3A, which also revealed a decreased averaged mEPSC amplitude in 5XFAD neurons. Pooled responses showed that 5XFAD neurons exhibited an overall lower amplitude of mEPSC (Fig. 3B), evidenced by both percentage distribution of the varying mEPSC amplitude bins, and the normalized cumulative distribution curve (number of mEPSC events: WT, n = 1244/12 cells/6 mice; 5XFAD, n = 1165/10 cells/5 mice. K-S test, D = 0.14, P <0.0001). In addition, 5XFAD neurons showed a significantly lower mEPSC frequency (Fig. 3C. Events/sec: WT, 3.72 ± 0.38; 5XFAD, 2.48 ± 0.28, P = 0.018). We next recorded miniature inhibitory postsynaptic currents (mIPSCs) in a different set of PFC slices, and found that mIPSC amplitude was largely unaltered in 5XFAD (Fig. 3D), as shown by the percentage and cumulative distribution across varying mIPSC amplitude bins (Fig. 3E. Number of mIPSCs analyzed: WT, n = 1244/7 cells/4 mice; 5XFAD, n = 1657/9 cells/5 mice. K-S test on cumulative distribution: D = 0.05, P = 0.79). Interestingly, we found a significant reduction of mIPSC frequency (Fig. 3F. Events/s: WT, 3.44 ± 0.32; 5XFAD, 2.23 ± 0.36. t_{18} = 2.54, P = 0.02). These data indicate alteration of both excitatory and inhibitory inputs onto PFC-L5 neurons in 5XFAD mice at an early post-weaning age.

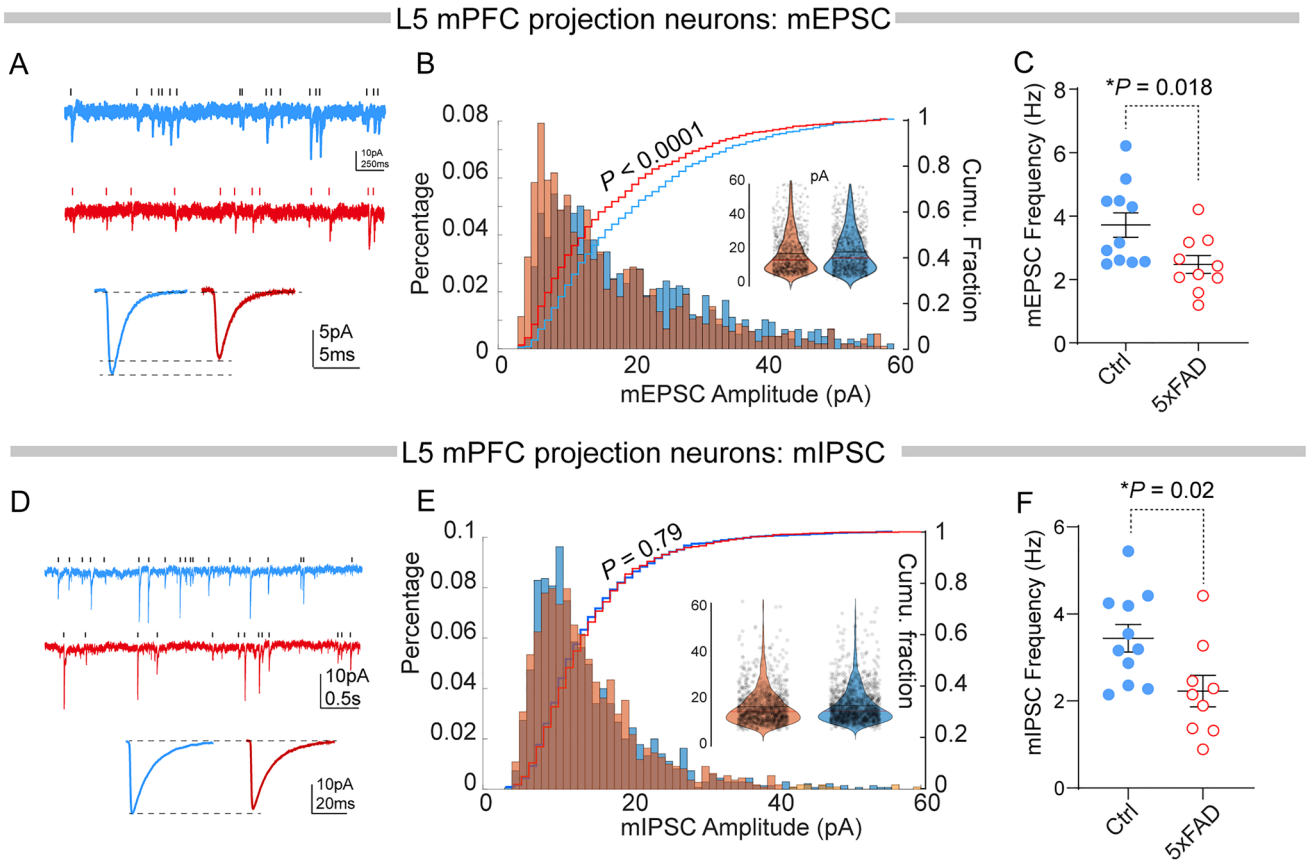

Fig. 3 Altered spontaneous synaptic mEPSC and mIPSC responses in PFC-L5 neurons at an early post-weaning age. **A** Representative whole-cell patch-clamp recording of spontaneous mEPSCs from 5XFAD and control neurons. **B** Quantification of all recorded mEPSC events. mEPSC amplitudes from 5XFAD neurons are distributed more to the smaller amplitude bins. There was also a significant difference between the cumulative distribution curves (K-S test, D = 0.14, ****P <0.0001). Inset, violin plot of pooled mEPSC amplitudes from both groups. **C** mEPSC frequency in 5XFAD PFC-L5 neurons is significantly reduced (*P = 0.018). **D** Representative traces of spontaneous mIPSCs from 5XFAD and control neurons. **E** 5XFAD and control neurons show a similar percentage distribution and cumulative distribution of all analyzed mIPSC amplitudes. No significant difference in the cumulative distribution curves was found (K-S test, P = 0.79). **F** 5XFAD neurons show a significant reduction in mIPSC frequency (t_{18} = 2.54, P = 0.02).

Decreased Dendritic Spine Size and Density in mPFC-L5 Neurons

We next asked whether the changes in synaptic responses have a morphological correlate. We analyzed anatomical changes of the dendritic structure and spines in PFC-L5 neurons from both WT and 5XFAD mice at P22–28. L5 neuron morphology was revealed by biocytin injection during whole-cell recording (Fig. 4A), followed by imaging of the dendritic structure and confocal Z-stack images of spines. Sholl analysis of dendritic arborization revealed that 5XFAD did not affect the number of dendritic intersections as a function of distance from the soma (Fig. 4B. Main group effect: $F_{(1, 15)} = 2.93$, $P = 0.11$, two-way ANOVA), nor did it affect the dendritic length distribution (Fig. 4C. Main group effect: $F_{(1, 15)} = 0.033$, $P = 0.86$, two-way ANOVA). However, 5XFAD neurons exhibited a reduced dendritic spine density (Fig. 4D, E. Number of spines/10 µm: WT, 12.52 ± 0.45; 5XFAD, 10.8 ± 0.37. $t_{21} = 2.89$, $P = 0.008$). In comparison, the spine length of 5XFAD neurons did not differ (Fig. 4F. Average length in µm: WT, 2.06 ± 0.13; 5XFAD, 2.20 ± 0.17. $t_{21} = 0.69$, $P = 0.49$). We next quantified the spine head volume and found that 5XFAD neurons showed a significant reduction (Fig. 4G. WT, n = 274 spines/6 neurons/6 mice; 5XFAD, n = 258 spines/7 neurons/5 mice. D = 0.286, P <0.0001, K-S test). These data were consistent with the decreased mEPSC amplitude and frequency, and further suggest impaired synaptic function in the PFC at a very early development age.

Altered Synaptic Glutamate Receptor Content in PFC-L5 Neurons

Considering that dendritic spine size and geometry are known to be correlated with glutamate receptor content and functional maturity [28], we asked whether PFC-L5 neurons

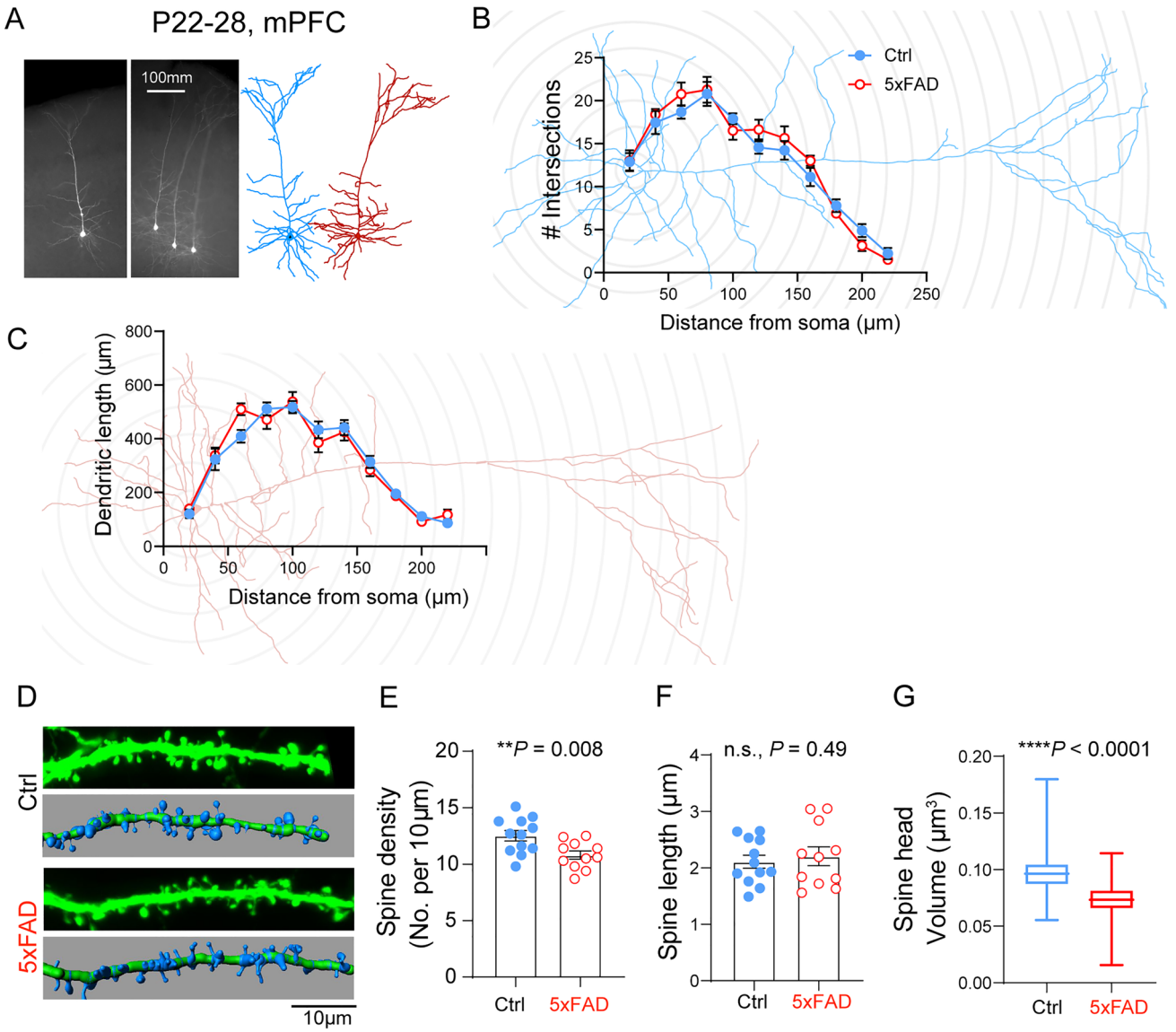

Fig. 4 Reduced dendritic spine size and density in PFC-L5 neurons in the early post-weaning period. **A** Dendritic morphology in L5 PFC neurons using avidin-Alexa 488 following whole-cell patch-clamp recordings. **B** Sholl analyses of the number of intersections of the PFC-L5 neuron dendritic arbors in control and 5XFAD neurons. No statistically significant differences if genotype were found ($P = 0.107$, two-way ANOVA. Note distal arbors are not included for analysis due to cutoff of some neurons. **C** Sholl analyses of dendritic length distribution. No significant difference was found for the dendritic length as a function of distance from soma between control and 5XFAD neurons ($F(1, 15) = 0.033$; $P = 0.86$ for main group effects). **D** Representative dendritic spines from control and 5XFAD PFC-L5 pyramidal neuron apical dendrites. **E** 5XFAD neurons show decreased spine density (**$P = 0.008$). **F** 5XFAD neurons do not differ in spine length ($P = 0.49$). **G** Cumulative distribution of spine head volume. Spine head volume from 5XFAD neurons is significantly reduced (****$P < 0.0001$, K-S test).

show changes of synaptic glutamate receptors. We first biotinylated the surface protein in parasagittal PFC slices, as described previously [29], then prepared crude synaptosome fractions using the biotinylated slices. Neutravidin beads were used to pull down the synaptic surface proteins. Total proteins were also probed using the crude synaptosome fraction without neutravidin pulldown (Fig. 5A). We found a significant reduction of AMPAR subunit GluA1 and the NMDA receptor subunit GluN2A. In comparison, the NMDA receptor subunit GluN2B was slightly increased. None of these changes, however, was observed using total synaptosome proteins (Fig. 5B). Quantification of these Western blot results (Fig. 5C) confirmed statistically significant decreases in GluA1 ($t_6 = 4.8$, $P = 0.003$) and GluN2A ($t_6 = 4.1$, $P = 0.007$). There was no statistical change in GluN1 ($t_6 = 0.41$, $P = 0.69$), but a marginal increase in GluN2B ($t_6 = 1.8$, P

= 0.12). These biochemical measures of synaptic glutamate receptor content further support the hypothesis that dendritic spine maturation is impaired at this age.

Impaired Functional Maturation of the PFC L2/3>L5 Circuits in 5XFAD Mice

Based on the changes in synaptic glutamate receptor content, we made whole-cell patch-clamp recordings to measure several parameters related to excitatory synapse maturation. PFC-L5 pyramidal neurons were first voltage-clamped at –70 mV, and monosynaptic responses to L23 stimulation were recorded. Neurons were then clamped at +40 mV to record compound AMPA/NMDA receptor responses. Quantification of pooled recordings revealed a significantly reduced AMPA/NMDA receptor current ratio (Fig. 6A. WT, 1.43 ± 0.06; 5XFAD, 1.16 ± 0.07. $t_{18} = 2.97$, $P = 0.008$), indicating impairment of synaptic transmission or synapse maturation. Cortical excitatory synapse maturation often entails activity-dependent AMPA receptor acquisition at synaptic sites that initially contain only NMDARs (silent synapses) [20, 30, 31] so that these synapses can be rendered functional. Impaired maturation can thus manifest as an increased number of silent synapses. Using a minimum stimulation protocol, we tested the proportions of silent synapses in WT and 5XFAD PFC-L5 neurons. A representative response to minimum stimulation from both groups of neurons at –70 mV and +40 mV holding potential is shown in Fig. 6B. Pooled data from multiple trials revealed that both WT and 5XFAD neurons showed an increased success rate of transmission (i.e., reduction in failure rate) at +40 mV compared to –70 mV (Fig. 6C). When failure rates were compared from all recorded neurons, it was found that 5XFAD neurons exhibited a larger difference in failure rates between the two holding potentials (Fig. 6D. WT, 17.5 ± 1.7; 5xFAD, 25.3± 2.9. $t_{14} = 2.26$, $P = 0.03$), confirming a higher proportion of immature silent synapses on 5XFAD PFC-L5 neurons.

Discussion

In this study, we present evidence on synaptic deficits in 5XFAD mice in the early post-weaning period that indicates altered intrinsic excitability, excitatory and inhibitory synaptic inputs, functional synapse maturation, and morphological perturbations in PFC projection neurons. Collectively, our data suggest the transgenic mutant APP/PS1 expression in a commonly studied AD mouse model [7, 32] perturbs the early developmental trajectory of the cortical circuit. The main focus was not to exhaustively pursue age-dependent pathological or electrophysiological changes, but rather to focus on L5 PFC neurons at a very early age and uncover potential circuit impairment using sensitive physiological and morphological measures. To the best of our knowledge, this study reports the earliest synaptic function and connectivity changes in 5XFAD mice in a major PFC projection neuron population. Our data demonstrate that mutant forms of APP/PS1 and likely the associated Aβ production [33] could have neurodevelopmental sequelae featuring disrupted early synapse development and maturation.

Our study also has a few limitations: first, only an early post-weaning age was examined, based on the early APP/Aβ overloading in the vulnerable L5 neuron population. It is unclear whether the synaptic pathology is transient, or persist and progress into adulthood. Second, the study focuses

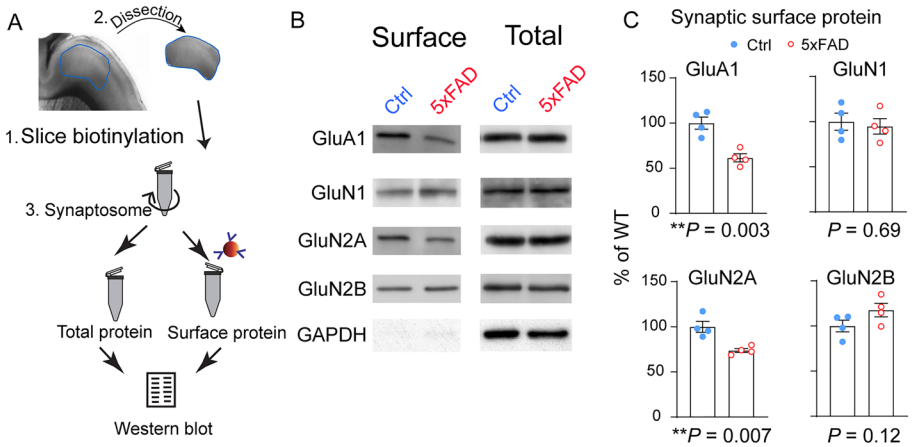

Fig. 5 Altered synaptic glutamate receptor content in 5XFAD L5 neurons (P22–28). **A** Schematic of dissecting PFC tissue after slice biotinylation, followed by crude synaptosome fraction preparation and synaptic surface protein isolation. **B** Representative Western blot results of synaptic surface and total synaptosome glutamate receptors: GluA1, GluN1, GluN2A, and GluN2B. **C** Quantification of Western blot results. 5XFAD PFC-L5 tissue shows reduced synaptic surface GluA1 (**$P = 0.003$) and GluN2A (**$P = 0.007$). There is a slight but non-significant increase in GluN2B ($P = 0.12$) and no difference in GluN1 ($P = 0.69$).

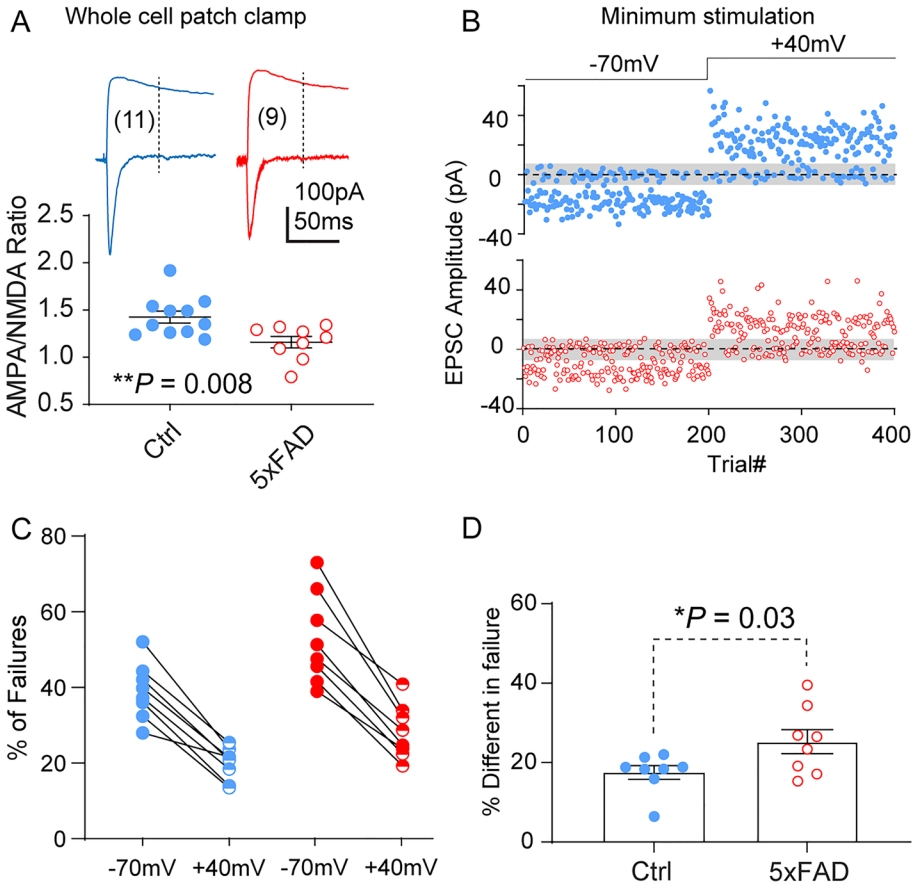

Fig. 6 5XFAD PFC-L5 neurons show a decreased AMPA/NMDA current ratio and increased number of silent synapses at P22–28. **A** AMPA/NMDA receptor current ratio is significantly reduced in 5XFAD neurons ($t_{18} = 2.97$, $^{**}P = 0.008$). **B** Representative responses of 5XFAD and control L5 neurons to consecutive trials in response to minimum stimulation of L2/3. Shaded patch centered on 0pA indicates RMS noise. Neurons had 200 trials at −70 mV holding potential followed by 200 trials at +40mV. **C** Quantification of failure rates at −70 mV and +40 mV holding potentials in control and 5XFAD neurons. **D** 5XFAD neurons exhibit a larger difference in failure rates between the two holding potentials ($^{*}P = 0.03$).

on one neuronal type and brain region, i.e., L5 neurons in the PFC. It is unclear how other neuronal types, the broader network activity, and even early behavior may be affected. Third, the implication of these findings on *adult* circuit function and age-dependent pathology remain to be studied. Nevertheless, our data indicate that certain circuit- and behavior-level deficits in adult and aging mice [7, 9, 34, 35] involve potential developmental perturbations in vulnerable neuronal populations, such as the L5 neurons across cortical regions.

Using immunohistochemical staining, we have shown that PFC-L5 neurons exhibit increased intracellular APP/Aβ loading at P21 (and earlier at P11–14, data not shown). Similarly, another vulnerable cortical population in terms of APP/Aβ overloading is the subiculum neurons of the temporal hippocampus, in which functional changes remain to be investigated at this age. Because the 6E10 antibody does not distinguish between APP and Aβ [36, 37], we cannot attribute these synaptic and circuit connectivity changes to APP or to intracellular Aβ production, which may be present at this age [33, 38]. Yet, our IHC staining revealed minimum microglial activation at P21, and there was no extracellular amyloid or dense-core fibrillar Aβ plaques in extracellular space. It is therefore less likely that physical loss of L5 neurons or synapses occurs at this early age. It has been reported that cortical L5 neurons are among the first neuronal populations that develop synaptic pathology [7, 9, 11], which is consistent with our recordings of decreased spontaneous mEPSC frequency and amplitude, a higher threshold for firing of APs, altered chemical composition of glutamate receptors, and increased silent synapses indicating less maturation at this early post-weaning age.

It is unclear how mutant APP/PS1 over-expression affects synaptic function in the developing brain and how the detrimental effects evolve with age. APP family members are posited to be involved in nervous system development, synaptogenesis, axon guidance and growth, formation of the neuromuscular junction, and establishing dendritic complexity and spines. They also contribute to synaptic functions, including synaptic plasticity, and learning and memory [39–42]. However, neurophysiological data exploring the effects of transgenic APP/PS1 on PFC circuit function are rather limited. Yet, the PFC is a primary and early target that develops AD pathology [43–45]. Transgenic mutant APP/PS1 in the developing cortical circuits may disrupt a myriad of physiological functions in neurons, including endo-lysosomal trafficking [46, 47], intracellular cargo transport [48], molecular signaling [49, 50], or neurotransmitter release [51] that collectively contribute to failure of synapse development and activity-dependent maturation.

In summary, our study revealed that synaptic function changes occur at an early post-weaning age in the 5XFAD mouse model. Our work supports the prevailing view of early intervention in AD at the cellular and circuit levels [52]. We provide detailed physiological characterization of PFC-L5 neurons, which is among the earliest affected cell types as a result of mutant APP/PS1. These functional disruptions suggest that transgenic mutant APP/PS1 overexpression has a profound effect on developing cortical circuits, and changes in neuronal function may instigate a life-long process that impacts neuronal degeneration at later ages. Therefore, although AD is considered a disease of old age, subtle neurological defects conferred by genetic mutations or risk factors may emerge early in life. This thought-provoking hypothesis justifies further studies to extend the limited scope of the current work.

Acknowledgements This work was supported by institutional startup funding from the University of Arizona (to SQ).

Data Availability The data used to support the findings of this study are available from the corresponding author upon reasonable request.

Conflict of interest The authors declare no conflict of interests.

References

1. De-Paula VJ, Radanovic M, Diniz BS, Forlenza OV. Alzheimer's disease. Subcell Biochem 2012, 65: 329–352.
2. Gómez-Isla T, Frosch MP. Lesions without symptoms: Understanding resilience to Alzheimer disease neuropathological changes. Nat Rev Neurol 2022, 18: 323–332.
3. Soria Lopez JA, González HM, Léger GC. Alzheimer's disease. Handb Clin Neurol 2019, 167: 231–255.
4. Ying Y, Wang JZ. Illuminating neural circuits in Alzheimer's disease. Neurosci Bull 2021, 37: 1203–1217.
5. Duyckaerts C, Potier MC, Delatour B. Alzheimer disease models and human neuropathology: Similarities and differences. Acta Neuropathol 2008, 115: 5–38.
6. Long X, Tao Y, Chen XC, Deng B, Cai J, Zhang SJ. Getting lost: Place cells and grid cells in rodent models of Alzheimer's disease. Neurosci Bull 2021, 37: 894–897.
7. Oakley H, Cole SL, Logan S, Maus E, Shao P, Craft J. Intraneuronal beta-amyloid aggregates, neurodegeneration, and neuron loss in transgenic mice with five familial Alzheimer's disease mutations: Potential factors in amyloid plaque formation. J Neurosci 2006, 26: 10129–10140.
8. Oh SJ, Lee HJ, Kang KJ, Han SJ, Lee YJ, Lee KC, *et al*. Early detection of A β deposition in the 5xFAD mouse by amyloid PET. Contrast Media Mol Imaging 2018, 2018: 5272014.
9. Richard BC, Kurdakova A, Baches S, Bayer TA, Weggen S, Wirths O. Gene dosage dependent aggravation of the neurological phenotype in the 5XFAD mouse model of Alzheimer's disease. J Alzheimers Dis 2015, 45: 1223–1236.
10. Kimura R, Ohno M. Impairments in remote memory stabilization precede hippocampal synaptic and cognitive failures in 5XFAD Alzheimer mouse model. Neurobiol Dis 2009, 33: 229–235.
11. Buskila Y, Crowe SE, Ellis-Davies GCR. Synaptic deficits in layer 5 neurons precede overt structural decay in 5xFAD mice. Neuroscience 2013, 254: 152–159.
12. Tible M, Mouton Liger F, Schmitt J, Giralt A, Farid K, Thomasseau S, *et al*. PKR knockout in the 5xFAD model of Alzheimer's disease reveals beneficial effects on spatial memory and brain lesions. PKR knockout in the 5xFAD model of Alzheimer's disease reveals beneficial effects on spatial memory and brain lesions. Aging Cell 2019, 18: e12887
13. Angel A, Volkman R, Royal TG, Offen D. Caspase-6 knockout in the 5xFAD model of Alzheimer's disease reveals favorable outcome on memory and neurological hallmarks. Int J Mol Sci 2020, 21: 1144.
14. Martorell AJ, Paulson AL, Suk HJ, Abdurrob F, Drummond GT, Guan W, *et al*. Multi-sensory gamma stimulation ameliorates Alzheimer's-associated pathology and improves cognition. Cell 2019, 177: 256-271.e22.
15. Seo J, Giusti-Rodríguez P, Zhou Y, Rudenko A, Cho S, Ota KT, *et al*. Activity-dependent p25 generation regulates synaptic plasticity and aβ-induced cognitive impairment. Cell 2014, 157: 486–498.
16. Feng G, Mellor RH, Bernstein M, Keller-Peck C, Nguyen QT, Wallace M, *et al*. Imaging neuronal subsets in transgenic mice expressing multiple spectral variants of GFP. Neuron 2000, 28: 41–51.
17. Bradley JE, Ramirez G, Hagood JS. Roles and regulation of Thy-1, a context-dependent modulator of cell phenotype. Biofactors 2009, 35: 258–265.
18. Qiu S, Anderson CT, Levitt P, Shepherd GMG. Circuit-specific intracortical hyperconnectivity in mice with deletion of the autism-associated Met receptor tyrosine kinase. J Neurosci 2011, 31: 5855–5864.
19. Terashima A, Pelkey KA, Rah JC, Suh YH, Roche KW, Collingridge GL, *et al*. An essential role for PICK1 in NMDA receptor-dependent bidirectional synaptic plasticity. Neuron 2008, 57: 872–882.
20. Liao D, Hessler NA, Malinow R. Activation of postsynaptically silent synapses during pairing-induced LTP in CA1 region of hippocampal slice. Nature 1995, 375: 400–404.
21. Qiu S, Lu Z, Levitt P. MET receptor tyrosine kinase controls dendritic complexity, spine morphogenesis, and glutamatergic synapse maturation in the hippocampus. J Neurosci 2014, 34: 16166–16179.
22. Qiu S, Weeber EJ. Reelin signaling facilitates maturation of CA1 glutamatergic synapses. J Neurophysiol 2007, 97: 2312–2321.
23. Qiu S, Zhao LF, Korwek KM, Weeber EJ. Differential reelin-induced enhancement of NMDA and AMPA receptor activity in the adult hippocampus. J Neurosci 2006, 26: 12943–12955.
24. Peng Y, Lu Z, Li G, Piechowicz M, Anderson M, Uddin Y, *et al*. The autism-associated MET receptor tyrosine kinase engages early neuronal growth mechanism and controls glutamatergic circuits development in the forebrain. Mol Psychiatry 2016, 21: 925–935.
25. Sholl DA. Dendritic organization in the neurons of the visual and motor cortices of the cat. J Anat 1953, 87: 387–406.
26. Longair MH, Baker DA, Armstrong JD. Simple Neurite Tracer: Open source software for reconstruction, visualization and analysis of neuronal processes. Bioinformatics 2011, 27: 2453–2454.
27. Herzig MC, Winkler DT, Burgermeister P, Pfeifer M, Kohler E, Schmidt SD, *et al*. Aβ is targeted to the vasculature in a mouse model of hereditary cerebral hemorrhage with amyloidosis. Nat Neurosci 2004, 7: 954–960.
28. Matsuzaki M, Ellis-Davies GCR, Nemoto T, Miyashita Y, Iino M, Kasai H. Dendritic spine geometry is critical for AMPA receptor expression in hippocampal CA1 pyramidal neurons. Nat Neurosci 2001, 4: 1086–1092.

29. Qiu S, Korwek KM, Pratt-Davis AR, Peters M, Bergman MY, Weeber EJ. Cognitive disruption and altered hippocampus synaptic function in Reelin haploinsufficient mice. Neurobiol Learn Mem 2006, 85: 228–242.
30. Huang YH, Lin Y, Mu P, Lee BR, Brown TE, Wayman G, *et al*. *In vivo* cocaine experience generates silent synapses. Neuron 2009, 63: 40–47.
31. Isaac JTR, Nicoll RA, Malenka RC. Evidence for silent synapses: Implications for the expression of LTP. Neuron 1995, 15: 427–434.
32. Holcomb L, Gordon MN, McGowan E, Yu X, Benkovic S, Jantzen P, *et al*. Accelerated Alzheimer-type phenotype in transgenic mice carrying both mutant amyloid precursor protein and presenilin 1 transgenes. Nat Med 1998, 4: 97–100.
33. William CM, Andermann ML, Goldey GJ, Roumis DK, Reid RC, Shatz CJ, *et al*. Synaptic plasticity defect following visual deprivation in Alzheimer's disease model transgenic mice. J Neurosci 2012, 32: 8004–8011.
34. Forner S, Kawauchi S, Balderrama-Gutierrez G, Kramár EA, Matheos DP, Phan J, *et al*. Systematic phenotyping and characterization of the 5xFAD mouse model of Alzheimer's disease. Sci Data 2021, 8: 270.
35. Oblak AL, Lin PB, Kotredes KP, Pandey RS, Garceau D, Williams HM, *et al*. Comprehensive evaluation of the 5XFAD mouse model for preclinical testing applications: A MODEL-AD study. Front Aging Neurosci 2021, 13: 713726.
36. Huwait EA, Baghallab IM, Glabe CG, Abulnaja KO, Kumosani TA, Moselhy SS. Identification of amyloid antibodies for Alzheimer disease-immunotherapy. Arch Physiol Biochem 2020, https://doi.org/10.1080/13813455.2020.1767147.
37. Droste P, Frenzel A, Steinwand M, Pelat T, Thullier P, Hust M, *et al*. Structural differences of amyloid-β fibrils revealed by antibodies from phage display. BMC Biotechnol 2015, 15: 57.
38. William CM, Stern MA, Pei X, Saqran L, Ramani M, Frosch MP, *et al*. Impairment of visual cortical plasticity by amyloid-beta species. Neurobiol Dis 2021, 154: 105344.
39. Benitez DP, Jiang S, Wood J, Wang R, Hall CM, Peerboom C, *et al*. Knock-in models related to Alzheimer's disease: Synaptic transmission, plaques and the role of microglia. Mol Neurodegener 2021, 16: 47.
40. Müller UC, Deller T, Korte M. Not just amyloid: Physiological functions of the amyloid precursor protein family. Nat Rev Neurosci 2017, 18: 281–298.
41. Probst S, Krüger M, Kägi L, Thöni S, Schuppli D, Nitsch RM, *et al*. Fe65 is the sole member of its family that mediates transcription regulated by the amyloid precursor protein. J Cell Sci 2020, 133: jcs242917.
42. Steubler V, Erdinger S, Back MK, Ludewig S, Fässler D, Richter M, *et al*. Loss of all three APP family members during development impairs synaptic function and plasticity, disrupts learning, and causes an autism-like phenotype. EMBO J 2021, 40: e107471.
43. Xu P, Chen A, Li Y, Xing X, Lu H. Medial prefrontal cortex in neurological diseases. Physiol Genomics 2019, 51: 432–442.
44. Bazzigaluppi P, Beckett TL, Koletar MM, Lai AY, Joo IL, Brown ME, *et al*. Early-stage attenuation of phase-amplitude coupling in the hippocampus and medial prefrontal cortex in a transgenic rat model of Alzheimer's disease. J Neurochem 2018, 144: 669–679.
45. Har-Paz I, Roisman N, Michaelson DM, Moran A. Extra-hippocampal learning deficits in young apolipoprotein E4 mice and their synaptic underpinning. J Alzheimers Dis 2019, 72: 71–82.
46. Kepp KP. Alzheimer's disease due to loss of function: A new synthesis of the available data. Prog Neurobiol 2016, 143: 36–60.
47. Maulik M, Peake K, Chung J, Wang Y, Vance JE, Kar S. APP overexpression in the absence of NPC1 exacerbates metabolism of amyloidogenic proteins of Alzheimer's disease. Hum Mol Genet 2015, 24: 7132–7150.
48. Bhalla A, Vetanovetz CP, Morel E, Chamoun Z, di Paolo G, Small SA. The location and trafficking routes of the neuronal retromer and its role in amyloid precursor protein transport. Neurobiol Dis 2012, 47: 126–134.
49. Xie CW. Calcium-regulated signaling pathways: Role in amyloid beta-induced synaptic dysfunction. Neuromolecular Med 2004, 6: 53–64.
50. Woods NK, Padmanabhan J. Neuronal calcium signaling and Alzheimer's disease. Adv Exp Med Biol 2012, 740: 1193–1217.
51. Ari C, Borysov SI, Wu J, Padmanabhan J, Potter H. Alzheimer amyloid beta inhibition of Eg5/kinesin 5 reduces neurotrophin and/or transmitter receptor function. Neurobiol Aging 2014, 35: 1839–1849.
52. Fan DY, Wang YJ. Early intervention in Alzheimer's disease: How early is early enough? Neurosci Bull 2020, 36: 195–197.